BEILSTEIN JOURNAL OF NANOTECHNOLOGY

Photocatalytic methane oxidation over a TiO_2/SiNWs p–n junction catalyst at room temperature

Qui Thanh Hoai Ta[1], Luan Minh Nguyen[1,2], Ngoc Hoi Nguyen[1,2], Phan Khanh Thinh Nguyen[*3] and Dai Hai Nguyen[*1,2]

Full Research Paper

Open Access

Address:
[1]Institute of Chemical Technology, Vietnam Academy of Science and Technology, 1A TL29 Street, Thanh Loc Ward, District 12, Ho Chi Minh City 700000, Vietnam, [2]Graduate University of Science and Technology, Vietnam Academy of Science and Technology, 18 Hoang Quoc Viet Street, Cau Giay District, Hanoi 100000, Vietnam and [3]Department of Chemical and Biological Engineering, Gachon University, 1342 Seongnamdaero, Sujeong-gu, Seongnam-si, Gyeonggi-do 13120, Republic of Korea

Email:
Qui Thanh Hoai Ta - tathanhhoaiqui2292@gmail.com;
Luan Minh Nguyen - nguyenminhluan.work@gmail.com;
Ngoc Hoi Nguyen - hoi83bmt@gmail.com;
Phan Khanh Thinh Nguyen* - thinhnpk@gachon.ac.kr;
Dai Hai Nguyen* - nguyendaihai0511@gmail.com

* Corresponding author

Keywords:
photocatalysis; photocatalytic CH_4 oxidation; p–n heterojunction; TiO_2/SiNWs

Beilstein J. Nanotechnol. **2024,** *15,* 1132–1141.
https://doi.org/10.3762/bjnano.15.92

Received: 18 May 2024
Accepted: 13 August 2024
Published: 02 September 2024

This article is part of the thematic issue "Recent advances in synthesis and applications of organometallic nanomaterials".

Guest Editor: B. T. Huy

Abstract

Rapid recombination of charge carriers in semiconductors is a main drawback for photocatalytic oxidative coupling of methane (OCM) reactions. Herein, we propose a novel catalyst by developing a p–n junction titania–silicon nanowires (TiO_2/SiNWs) heterostructure. The structure is fabricated by atomic layer deposition of TiO_2 on p-type SiNWs. The TiO_2/SiNWs heterostructure exhibited an outstanding OCM performance under simulated solar light irradiation compared to the single components. This enhanced efficiency was attributed to the intrinsic electrical field formed between n-type TiO_2 and p-type SiNWs, which forces generated charge carriers to move in opposite directions and suppresses charge recombination. Besides, surface morphology and optical properties of the the p–n TiO_2/SiNWs catalyst are also beneficial for the photocatalytic activity. It is expected that the results of this study will provide massive guidance in synthesizing an efficient photocatalyst for CH_4 conversion under mild conditions.

Introduction

Methane (CH_4), which can take the form of liquefied natural gas, is one of the crucial sources of industrial chemicals and energy. However, CH_4 is a major precursor for tropospheric ozone, causing severe air pollution. Because of its rising atmospheric concentration, CH_4 poses a global warming potential approximately thirty fold larger than that of carbon dioxide

(CO_2) [1-3]. Therefore, it is a challenging mission to eliminate CH_4 from the atmosphere. Conventionally, CH_4 activation is carried out at high temperatures (>650 °C) via thermal methane conversion to value-added products. However, combustion of CH_4 for energy production usually generates great amounts of carbon dioxide as well as coke deposition on catalyst surfaces [4-7]. Therefore, sustainable strategies for both green conversion and atmospheric removal of CH_4 are urgently necessary [8-11]. Semiconductor-based photocatalysis has been attracting scientists' attention because of its environmental friendliness and easy handling [12-14]. Photocatalytic metal oxide semiconductor materials have been utilized for converting solar energy into valuable chemical energy in the field of CH_4 conversion [15-17]. Methane oxidation presents a particularly promising strategy. The primary objective is to convert methane into valuable products such as formaldehyde (HCHO), methanol (CH_3OH), and other value-added oxygenates, which serve as essential precursors in various manufacturing and production processes [18,19].

The n-type semiconductor titanium dioxide (TiO_2) has been discovered as a potential photocatalyst material because of its high stability, good dispersibility, and narrow energy bandgap. However, pristine TiO_2 shows only low photocatalytic efficiency because of the high recombination rate between holes and electrons and the low visible-light harvesting ability [20-22]. The rapid recombination of charge carriers prior to their participation in reactions significantly reduces the efficiency of methane oxidation reactions [23,24]. To address these issues of TiO_2 nanomaterials, many scientists have developed TiO_2-based nanostructure composites as advanced photocatalysts [25-30]. The recombination of charge carriers is mainly attributed to the anisotropic movement of generated electron–hole pairs in semiconductors. Therefore, the implementation of a driving force could remarkably accelerate the oriented motion of electrons and holes, which could suppress recombination and eventually improve photocatalytic efficiency. For years, doping of metal nanoparticles (NPs) into a semiconductor matrix has been extensively studied to enhance photocatalytic CH_4 oxidation performance. Metal NPs in, for example, Au/TiO_2, Au@Pd/ZnO, and Pt@Cu/TiO_2 composites act as electron scavenger centers and own more free electrons for reactions [25-27]. However, the generated electron affinity of metal NPs is sometimes insufficient and cannot prevent recombination or maintain electrons for further reactions.

As an advanced solution for catalysis modification, p–n junction photocatalysts with an intrinsic electric field formed at the interface have emerged, which effectively force charge carriers to move in opposite directions and hinder recombination [31-33]. Very recently, $Cu_2O/BiVO_4$, $Ag_2O/Bi_{12}O_{17}Cl_2$ and $CuFe_2O_4/Bi_4Ti_3O_{12}$ composite powders have shown improved efficiencies in water treatment based on p–n configuration advantages [34-36]. However, the wetness impregnation synthesis of those powder co-catalysts faces the issues of low surface area, low reproducibility, and difficult control of large-scale production. Therefore, the development of novel catalysts with unique morphologies by using precise tools is extremely essential and important [37-39].

Herein, we constructed a robust p–n junction catalyst by atomic layer deposition (ALD) of TiO_2 thin films on a p-type SiNW substrate for enhancing the photocatalytic efficiency in CH_4 oxidation. Pristine p-Si wafers have limited surface area and are highly susceptible to mechanical failure because of their brittle nature; in contrast, the etched SiNW arrays exhibit superior optical absorption and enhanced surface catalytic reaction properties. The intimate contact between 1D Si NWs and thin TiO_2 layers reduces the recombination rate of electron–hole pairs. Additionally, TiO_2/SiNWs offer flexibility, improved bandgap energy, and enhanced light harvesting across a broad spectrum, leading to higher photocatalytic efficiency. Combining SiNWs and TiO_2 presents an opportunity to leverage the strengths of both materials while mitigating their respective limitations. This study offers new insights into the design of an efficient system for OCM.

Results and Discussion

Structural and morphological properties

For understanding the crystalline structure of TiO_2 and SiNWs, X-ray diffraction patterns were recorded as displayed in Figure 1. The XRD pattern of a pure Si wafer and p-type SiNWs display a main peak at 2θ of 33.2°, which was attributed to the reflection from (200) planes. Despite being etched with concentrated acid and Ag^+ ions, there was no significant

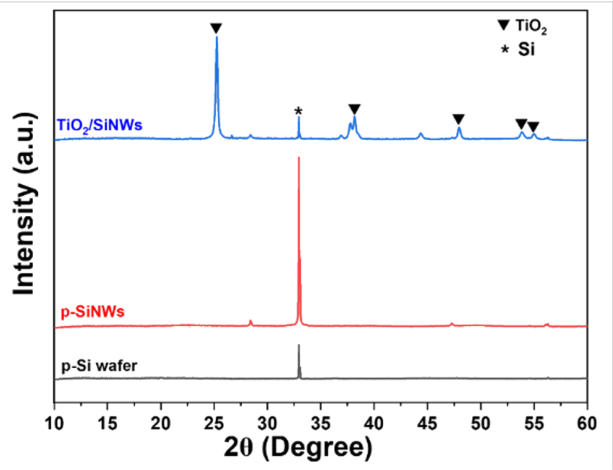

Figure 1: XRD patterns of p-Si, p-type SiNWs, and the TiO_2/SiNWs sample.

change in the peak position of p-type SiNWs, which corresponds to the original Si phase (JCPDS No.27-1402) [40,41]. In the case of the as-synthesized composite, the favored growth of TiO_2(101) on the surface of p-Si NWs has been noticed [42]. The minor (112), (200), (105), and (211) peaks at 2θ = 38.2°, 48.5°, 53.3°, and 55.1° indicate the formation of anatase TiO_2 (JCPDS No.21-1272) [43,44]. As expected, the crystal orientation of the TiO_2/SiNWs catalyst obviously led to the creation of a robust p–n junction photocatalyst.

The SEM analysis further confirms the morphological evolution during etching and TiO_2 ALD. As revealed in Supporting Information File 1, Figure S1, the morphology of SiNWs is characterized by individual nanowires that bunch together in a highly ordered manner, resulting in well-oriented Si NW arrays perpendicular to the Si bulk surface. Figure 2 shows cross-sectional- and top-view SEM images of the as-prepared TiO_2/SiNWs sample. The TiO_2/SiNWs arrays were well prepared with an average length of 4 µm. Moreover, the surface of the SiNWs was fully decorated by the TiO_2 passivation layer and became blurry. The active pure 25 nm TiO_2 layer exhibits flake-like morphology as displayed in Figure 2c,d.

Optical properties

Nanowire arrays offer a better optical absorption than planar Si wafers because of the specific morphology [45]. The optical absorption of the as-prepared catalyst is shown in Figure 3a. The UV–vis diffuse reflection spectrum of TiO_2/SiNWs catalyst is drastically reduced in comparison to the pure SiNWs. The superior antireflection property of the TiO_2/SiNWs catalyst may be attributed to the vertical wires, which enable strong light scattering leading to enhancement in light harvesting. The optical bandgap values of SiNWs and TiO_2/SiNWs are estimated at around 3.8 and 3.3 eV, respectively. Figure 3b displays the current–voltage (*I*–*V*) curves of the photocatalyst under dark and light conditions. The current of the sample under light conditions is higher than that under dark conditions. The slope of the *I*–*V* characteristic starts to increase, showing that generated electrons strongly influence the electrical properties of the samples.

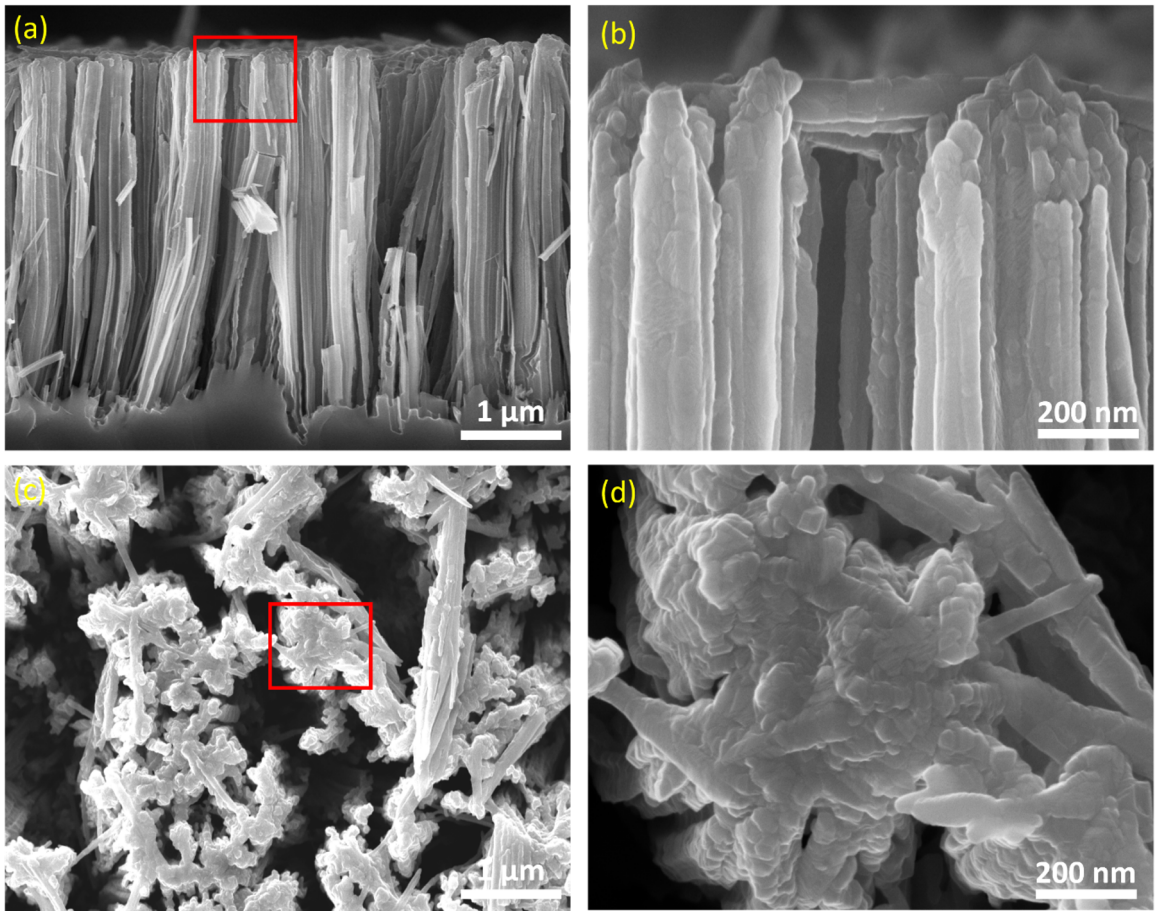

Figure 2: Cross-sectional view (a, b) and top view (c, d) SEM images of the TiO_2/SiNWs device with a higher-magnification view of the red rectangles on the right-hand side. A thin layer of TiO_2 (estimated at 25 nm) was deposited on the SiNWs by using ALD with 500 deposition cycles.

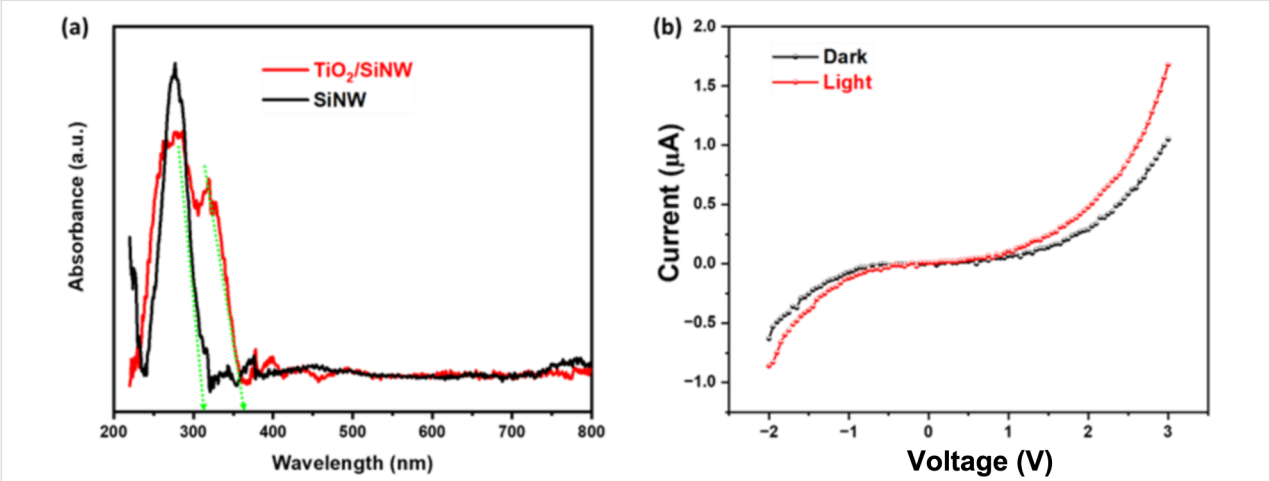

Figure 3: The UV–visible diffuse reflectance spectra (a) and *I–V* curve under light/dark conditions (b) of the TiO_2/SiNWs sample.

The surface interaction with gases during photocatalytic oxidative coupling can be analyzed using water contact angle analysis (as shown in Supporting Information File 1, Figure S2). The wettability of pure p-Si and the p-Si NW array are illustrated in Figure S3 (Supporting Information File 1). Pure p-Si had a water contact angle of 50.24°. Because of the nanowire array morphology, the p-Si NWs were more hydrophilic nature with a water contact angle of 3.36°, which manifests superior photocatalytic oxidative coupling.

Raman spectra were conducted to confirm the surface composition of the synthesized photocatalysts. As depicted in Figure 4a, the Raman spectrum of Si exhibits a single peak located at 519 cm^{-1}, corresponding to the first-order transverse optical (TO) mode of Si [46]. For the TiO_2/Si photocatalyst, two distinct peaks were observed, namely, (i) the characteristic E_g vibration of TiO_2, located at 146 cm^{-1}, and (ii) the TO phonon mode of Si (Figure 4b) [47-49]. Consequently, the combined surface-sensitive Raman and bulk-sensitive XRD results reveal that the n-type TiO_2 coating layer on p-type SiNWs does not influence the crystalline structure.

Photocatalytic OCM

The photocatalytic OCM activity of TiO_2/SiNWs sample under aerobic conditions is described in Figure 5. In a batch reactor, the photocatalytic CH_4 oxidation progresses as a function of irradiation time. Besides ethane (C_2H_6), carbon dioxide (CO_2) was detected as a by-product. Moreover, propane (C_3H_8) and H_2 were observed as result of the oxidative cross-coupling of methane and ethane (Figure 5a). The conversion reaction of CH_4 can be described as follows:

$$2CH_4 \rightarrow C_2H_6 + H_2.$$

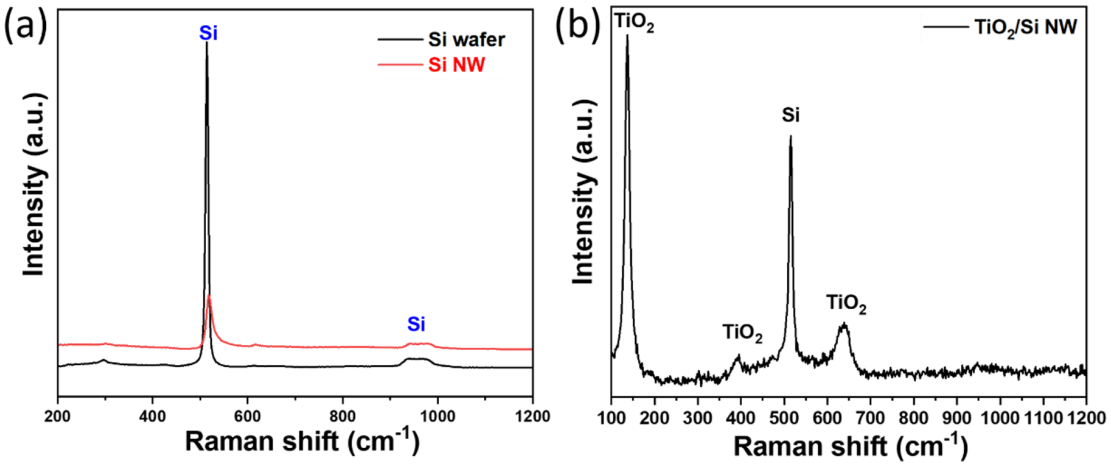

Figure 4: Raman spectra of pure p-Si and Si NW (a), and the TiO_2/SiNWs thin film (b).

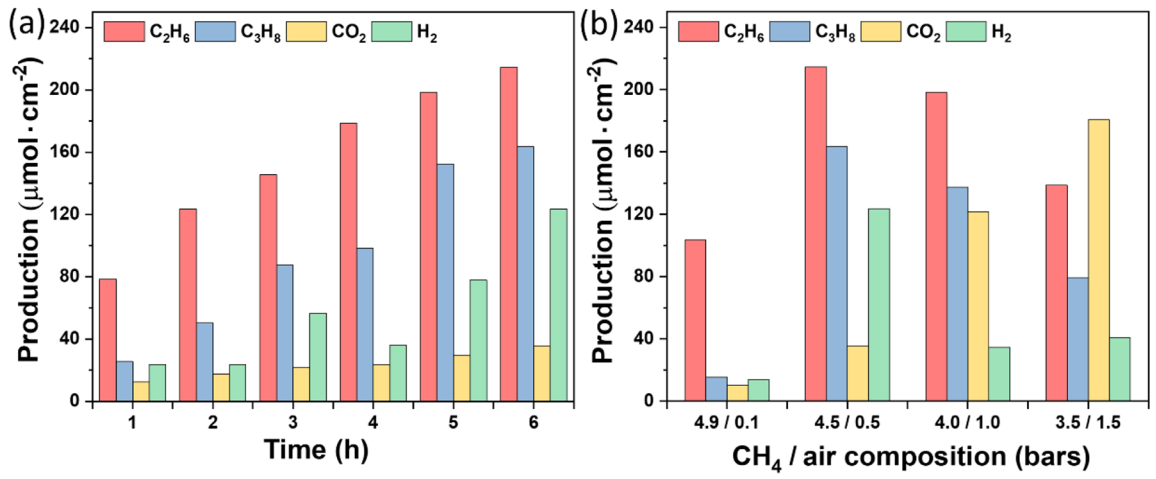

Figure 5: Photocatalytic CH_4 oxidation as a function of irradiation time (a) and different CH_4/air composition (b) over TiO_2/SiNWs. Reaction conditions: TiO_2/SiNWs chip (1 × 2 cm^2), total pressure of 5 bar, 20 °C, reaction time t = 6 h in (b).

To evaluate the reaction ratio-dependent photocatalytic OCM efficiency, we varied the gas pressure ratios between CH_4 and air. As shown in Figure 5b, more CO_2 was measured at lower CH_4-to-air ratios because of the higher O_2 content. Therefore, optimizing the CH_4/air ratio is important for improving the OCM reaction. The highest coupling selectivity was around 90% at CH_4/air ≈ 4.5:0.5, comparable to or higher than that of typical reported photocatalysts (Table 1). Although the TiO_2/Si composite did not achieve the best results compared to other photocatalysts, it remains a viable option for methane oxidation processes.

In order to investigate the individual effects of p-type SiNWs and TiO_2 layer on the photocatalytic OCM efficiency, comparable samples were irradiated under the same conditions. The methane coupling was analyzed with different samples using pure p-type SiNW, TiO_2/SiNW, TiO_2/glass catalyst, as shown in Figure 6a. In fact, only negligible CH_4 conversion was discovered over p-type SiNWs, and TiO_2/glass under the same conditions. It can be explained that the superior wettability of TiO_2/SiNWs (hydrophilic surfaces) compared to TiO_2/glass (hydrophobic surfaces) enables partial adsorption of water molecules, which facilitates the generation of radicals necessary for photocatalytic reactions. Furthermore, the TiO_2 nanostructure and p-type SiNWs are crucial in photogenerated charge separation and adsorption enhancement under UV–vis light. In other words, the ethane productivity of TiO_2/Si NWs was five times higher (210 μmol/cm^2) than that of pure p-Si NWs (20 μmol/cm^2) and glass/TiO_2 (30 μmol/cm^2).

Photocatalytic OCM over TiO_2/Si NWs catalysts was recorded in a batch reactor under different wavelengths of light. As

Table 1: Comparison of the OCM performance of the TiO_2/Si composite with previous photocatalysts.

Photocatalysts	Amount of catalyst	Reaction conditions	Light	Productivity (μmol·g^{-1}·h^{-1}) and selectivity	Ref.
Au@$Zn_2Ti_3O_8$	0.03 g	CH_4/O_2 = 15:1, mild conditions	50 W LED	C_2H_6: 1219 Sel.: 81%	[50]
Pt@TiO_2	0.075 g	CH_4 and water	UV lamp	C_2H_6: 57 Sel.: 62%	[51]
AuZnO@TiO_2	0.02 g	CH_4/air = 69:1, mild conditions	300 W Xe lamp	C_2H_6: 5020 Sel.: 90%	[30]
Ag HPW@TiO_2	0.1 g	CH_4 and air, 0.3 MPa	400 W Xe lamp	C_2H_6: 21 Sel.: 90%	[52]
Au@ZnO	0.005 g	CH_4/O_2 = 99:1, mild conditions	2 LEDs	C_2-C_4:684 Sel.: 83%	[53]
TiO_2/Si	1 × 2 cm^2	CH_4/air = 4.5:0.5, 0.5 MPa	300 W Xe lamp	C_2H_6: 210 μmol/cm^2 in 6 h Sel.: 90%	this work

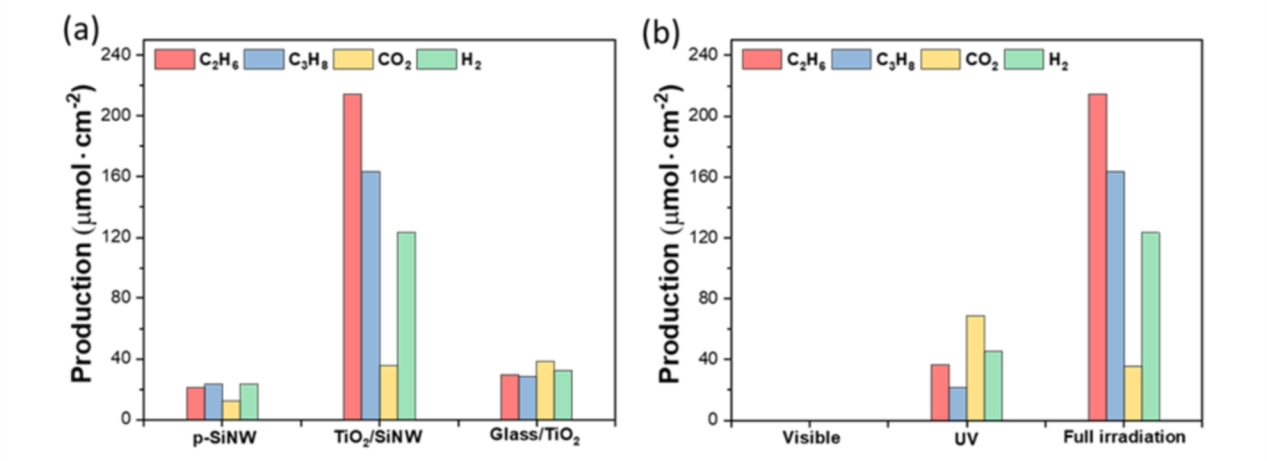

Figure 6: Photocatalytic CH_4 oxidation over different types of catalyst (a), and under different types of irradiation (b). Note that only TiO_2/SiNWs was used in panel (b). Reaction conditions: 5 bar, 20 °C, t = 6 h.

shown in Figure 6b, no products were detected under the visible-light irradiation. The photocatalytic performance under UV illumination was significantly lower than that under full illumination.

Figure 7 shows the recyclability of the p–n TiO_2/SiNWs photocatalyst. Note that after each cycle, the reactor was completely evacuated, and fresh gases were refilled for the following run. The photocatalytic activity of p–n TiO_2/SiNWs remained almost unchanged after four consecutive reaction cycles, indicating a high recyclability in the batch reactor.

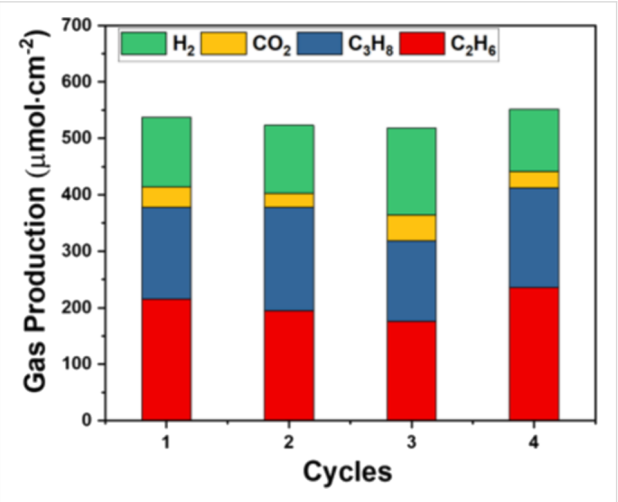

Figure 7: Stability of photocatalytic CH_4 oxidation reaction over the TiO_2/SiNWs sample.

Plausible charge transport mechanism

Figure 8 shows a schematic mechanism of the photocatalytic activity of the p–n TiO_2/SiNWs hierarchical structures. According to previous studies the energy bandgaps of p-Si and n-type TiO_2 were assumed to be 1.1 eV and 3.3 eV, respectively [54-56]. Because of the different electron affinities ($E_{ea,TiO2} \approx 4.10$ eV, $E_{ea,Si} \approx 4.05$ eV) [57,58] the electrons are excited and moved from the valance band minimum (VBM, 0.74V vs NHE) of SiNWs to the conduction band maximum (CBM, 0.35V vs NHE) of TiO_2 to enter the equilibrium state under irradiation following Aderson's model [39]. The photogenerated electrons tend to produce C_2H_6, C_3H_8, and H_2 from H^+. The photogenerated holes at the VBM of TiO_2 create oxidized intermediates and H^+ [59-61]. The whole process can be expressed by the S-scheme mechanism, as follows:

$$TiO_2/\text{Si NWs} \rightarrow TiO_2\left(h^+ + e^-\right) + \text{Si NWs}\left(h^+ + e^-\right),$$

at the CB of n-type TiO_2

$$O_2 + e^- + C^{\cdot} \rightarrow CO_2,$$

and at the VB of p-Si NW

$$CH_4 + h^+ \rightarrow H^+ + CH_2^{\cdot} + CH_3^{\cdot} + C^{\cdot} \rightarrow H_2 + C_2H_6 + C_3H_8.$$

Conclusion

A p–n junction TiO_2/SiNWs photocatalyst was synthesized via ALD and utilized for light-driven OCM. TiO_2/SiNWs revealed excellent performance owing to the smooth transport of photogenerated electrons in the p–n junction, which lowers the e–h recombination rate. The nanowire array structure of the catalyst provides a surface that can massively increase light absorption, achieving an efficient C_2H_6 yield of 210 μmol/cm^2 in 6 h with high selectivity under light illumination at room temperature. This research could offer new insights into composite photocatalysts for methane coupling.

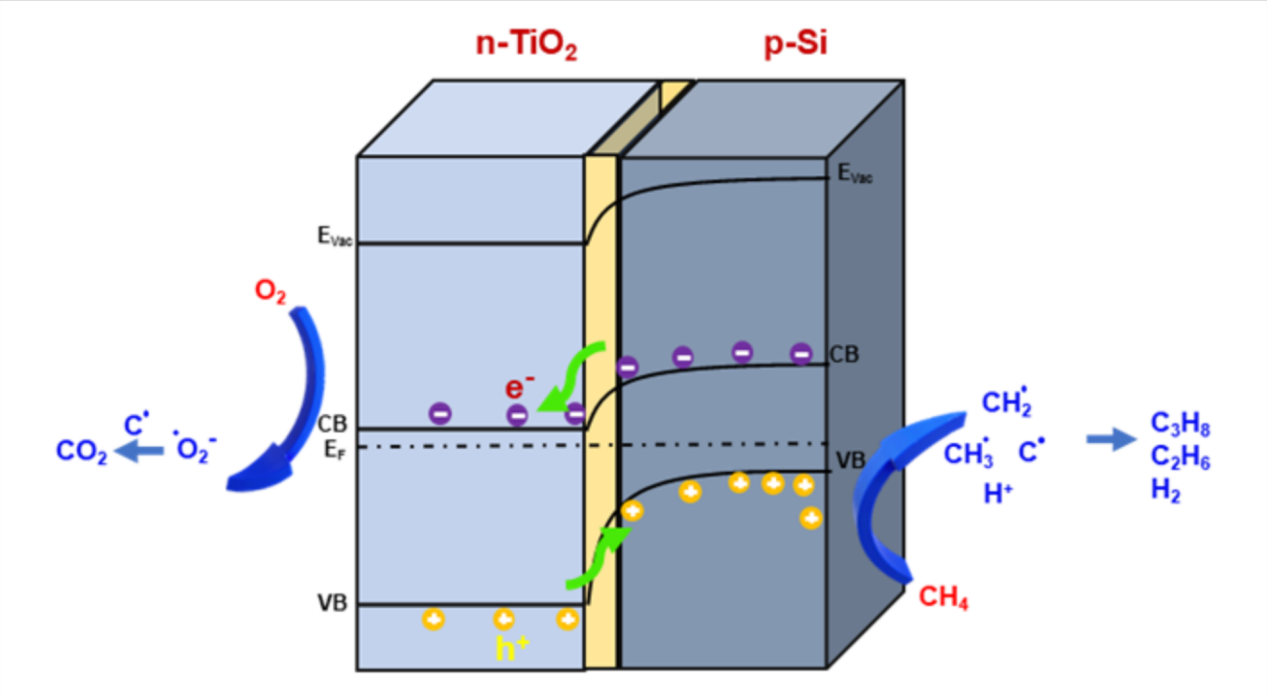

Figure 8: Proposed mechanism of photocatalytic CH_4 oxidation reaction over p–n junction TiO_2/SiNWs sample.

Experimental

Chemicals and materials

Commercial p-type Si 3-inch wafers (⟨100⟩ orientation, boron-doped, resistivity = 0.01–1 Ω·cm) were purchased from Silicon Mitus Corporation, South Korea. Silver nitrate ($AgNO_3$, 0.1 M), hydrofluoric acid HF (50 wt %), nitric acid (HNO_3, 63%), acetone, and ethanol were provided from Sigma-Aldrich. Deionized (DI) water was used for cleaning steps.

Si NWs and TiO_2/Si NWs preparation

First, a small piece (1 × 2 cm^2) was cut from a commercial p-type Si wafer and washed several times using DI water, ethanol, and acetone in a sonication bath. Etching solution containing $AgNO_3$ (0.1 M), HF (50 wt %) and H_2O (2:1:2 vol %) was prepared and kept at 56 °C for 20 min. The clean Si substrate was rapidly immersed in the etching medium and etched by the Ag^+ ions for 25 min to obtain 4 μm long SiNWs. Afterwards, remaining Ag on the Si surface was removed using HNO_3 (63 wt %) for 10 min. The etched p-Si NWs substrate was eventually washed with DI water and dried under N_2 flow, as shown in Figure 9.

Second, the as-prepared SiNWs sample was transferred to the chamber of an ALD system (R200 Advanced Picosun, 2013) for TiO_2 thin film deposition. The TiO_2 thin film deposition was carried out at 300 °C using $TiCl_4$ (98% purity, 0.2 s pulse time) and H_2O (0.1 s pulse time) as precursors. The vacuum level of

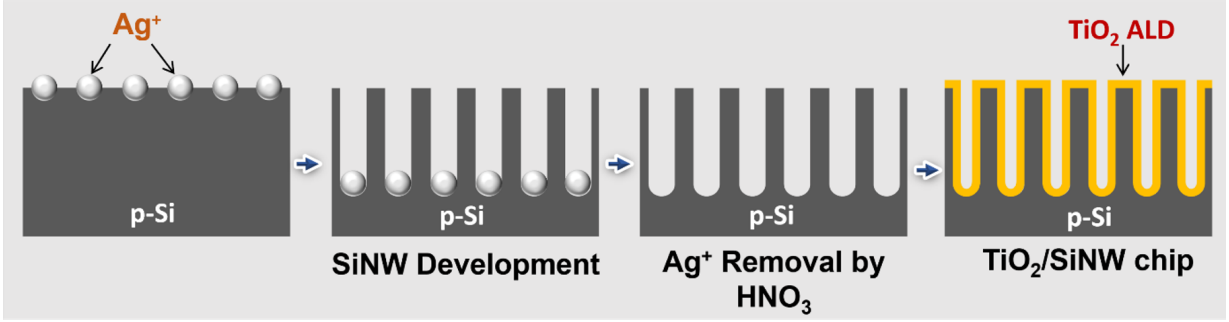

Figure 9: Schematic illustration of TiO_2/SiNWs chip fabrication starting from a p-type silicon wafer. A thin layer of TiO_2 was deposited on the Si NWs via ALD.

the chamber was kept at 8×10^{-3} bar, and the deposition rate was 0.051 nm/cycle. After cooling down to room temperature, the sample was taken out from chamber for photocatalytic experiments.

Photocatalytic tests

The as-synthesized catalyst was placed in a custom-made batch reactor with a small transparent quartz window, which was directly connected to a gas chromatograph (GC) with thermal conductivity and flame ionization detectors. A 300 W Xenon lamp was utilized as a light source (HAL-320). First, the reactor containing the photocatalytic thin film samples was evacuated using a vacuum pump for 10 min and filled with a mixture of CH_4/air (4.5/0.5 pressure ratio). The pressure ratio of the gas mixture was varied to study gas composition-dependent efficiency. The total pressure of gaseous reactants in batch reactor was established at 5 bar, and the photocatalytic system was kept in the dark (20 min) to reach equilibrium before exposure to simulated solar light. The temperature was kept at room temperature via a cooler.

Characterization

The crystalline structure and morphological properties of as-synthesized samples were analyzed using an X-ray diffraction system (XRD, Rigaku, SmartLab) with a 2θ range of 20–80° and a field-emission scanning electron microscope (FE-SEM, Hitachi, S-4700). The absorption properties of the thin films were analyzed using a diffuse reflectance UV–vis spectrometer (DRS-UV, Shimazu UV-2450). The chemical structure of the catalyst surface was analyzed using a Raman spectrometer (excitation of 532 nm, ANDOR Monora 500i). The surface wettability of the thin film sample was measured using a static contact angle system (Biosin Scientific), as shown in Supporting Information File 1, Figure S2. The contact angle between horizontal sample surface and the perimeter of the water drop was measured after 10 s of interaction. The in situ photocurrent measurements were carried out in the presence of gaseous reactants (CH_4/air = 4.5/0.5) ranging from −2 V to +3 V under dark and light conditions. Each measurement was scanned with 0.05 V intervals. The bias supply and current signals were provided and recorded by a Keithley system adapted with an amplifier.

Supporting Information

Supporting Information File 1

Additional figures.
[https://www.beilstein-journals.org/bjnano/content/supplementary/2190-4286-15-92-S1.pdf]

Acknowledgements

We acknowledge Material projects for using the TiO_2 and Si CIF files for the structures in the graphical abstract. The TiO_2 structure was reproduced from https://next-gen.materialsproject.org/materials/mp-1215, and the Si structure was reproduced from https://next-gen.materialsproject.org/materials/mp-165 (both published by The Materials Project and distributed under the terms of the Creative Commons Attribution 4.0 International License, https://creativecommons.org/licenses/by/4.0). Both structures were combined using the Vesta software (Momma, K.; Izumi, F. *J. Appl. Crystallogr.* **2011,** *44,* 1272–1276).

Funding

Ta Thanh Hoai Qui was funded by the Postdoctoral Scholarship Programme of Vingroup Innovation Foundation (VINIF), code VINIF.2023.STS.62.

Competing Interest

The authors declare that they have no known competing financial interests or personal relationships that could have appeared to influence the work reported in this paper.

Author Contributions

Qui Thanh Hoai Ta: supervision; validation; visualization; writing – original draft. Luan Minh Nguyen: data curation; formal analysis. Ngoc Hoi Nguyen: resources; software. Phan Khanh Thinh Nguyen: supervision; validation; visualization. Dai Hai Nguyen: writing – original draft; writing – review & editing.

ORCID® iDs

Qui Thanh Hoai Ta - https://orcid.org/0000-0002-0387-6281
Luan Minh Nguyen - https://orcid.org/0000-0003-3981-2084
Phan Khanh Thinh Nguyen - https://orcid.org/0000-0002-8204-6701
Dai Hai Nguyen - https://orcid.org/0000-0003-3501-7390

Data Availability Statement

The data that supports the findings of this study is available from the corresponding author upon reasonable request.

References

1. Reay, D.; Smith, P.; van Amstel, A. Methane Sources and the Global Methane Budget. In *Methane and Climate Change,* 1st ed.; Reay, D.; Smith, P., Eds.; Routledge: Abingdon-on-Thames, United Kingdom, 2010; pp 1–13. doi:10.4324/9781849775090
2. Lai, D. Y. F. *Pedosphere* **2009,** *19,* 409–421. doi:10.1016/s1002-0160(09)00003-4
3. Van Amstel, A. *J. Integr. Environ. Sci.* **2012,** *9,* 5–30. doi:10.1080/1943815x.2012.694892
4. Zamri, A. A.; Ong, M. Y.; Nomanbhay, S.; Show, P. L. *Environ. Res.* **2021,** *197,* 111204. doi:10.1016/j.envres.2021.111204

5. Biernat, K.; Malinowski, A.; Gnat, M. *The Possibility of Future Biofuels Production Using Waste Carbon Dioxide and Solar Energy;* Biofuels - Economy, Environment and Sustainability; InTech: Rijeka, Croatia, 2013. doi:10.5772/53831
6. Soeder, D. J. *Adv. Geo-Energy Res.* **2021,** *5,* 274–285. doi:10.46690/ager.2021.03.04
7. Benson, S. M. In *Carbon Dioxide Capture for Storage in Deep Geologic Formations – Results from the CO2 Capture Project: Vol 1-Capture and Separation of Carbon Dioxide from Combustion, Vol 2-Geologic Storage of Carbon Dioxide with Monitoring and Verification;* Thomas, D. C., Ed.; Elsevier, 2005. doi:10.1016/b978-008044570-0/50126-4
8. Mar, K. A.; Unger, C.; Walderdorff, L.; Butler, T. *Environ. Sci. Policy* **2022,** *134,* 127–136. doi:10.1016/j.envsci.2022.03.027
9. Collins, W. J.; Webber, C. P.; Cox, P. M.; Huntingford, C.; Lowe, J.; Sitch, S.; Chadburn, S. E.; Comyn-Platt, E.; Harper, A. B.; Hayman, G.; Powell, T. *Environ. Res. Lett.* **2018,** *13,* 054003. doi:10.1088/1748-9326/aab89c
10. Song, H.; Meng, X.; Wang, S.; Zhou, W.; Wang, X.; Kako, T.; Ye, J. *J. Am. Chem. Soc.* **2019,** *141,* 20507–20515. doi:10.1021/jacs.9b11440
11. Jiang, Y.; Li, S.; Wang, S.; Zhang, Y.; Long, C.; Xie, J.; Fan, X.; Zhao, W.; Xu, P.; Fan, Y.; Cui, C.; Tang, Z. *J. Am. Chem. Soc.* **2023,** *145,* 2698–2707. doi:10.1021/jacs.2c13313
12. Zhu, J.; Liao, M.; Zhao, C.; Liu, M.; Han, A.; Zhu, C.; Sun, Y.; Zhao, M.; Ye, S.; Cao, H. *Nano Res.* **2023,** *16,* 6402–6443. doi:10.1007/s12274-023-5428-6
13. Kim, C.-M.; Jaffari, Z. H.; Abbas, A.; Chowdhury, M. F.; Cho, K. H. *J. Hazard. Mater.* **2024,** *465,* 132995. doi:10.1016/j.jhazmat.2023.132995
14. Mao, J.; Ta, Q. T. H.; Tri, N. N.; Shou, L.; Seo, S.; Xu, W. *Appl. Mater. Today* **2023,** *35,* 101939. doi:10.1016/j.apmt.2023.101939
15. Baharudin, L.; Rahmat, N.; Othman, N. H.; Shah, N.; Syed-Hassan, S. S. A. *J. CO2 Util.* **2022,** *61,* 102050. doi:10.1016/j.jcou.2022.102050
16. Zhou, Z.; Sun, Z.; Duan, L. *Curr. Opin. Green Sustainable Chem.* **2023,** *39,* 100721. doi:10.1016/j.cogsc.2022.100721
17. Taifan, W.; Baltrusaitis, J. *Appl. Catal., B* **2016,** *198,* 525–547. doi:10.1016/j.apcatb.2016.05.081
18. Tucci, F. J.; Rosenzweig, A. C. *Chem. Rev.* **2024,** *124,* 1288–1320. doi:10.1021/acs.chemrev.3c00727
19. Siang, T. J.; Jalil, A. A.; Liew, S. Y.; Owgi, A. H. K.; Rahman, A. F. A. *Catal. Rev.: Sci. Eng.* **2024,** *66,* 343–399. doi:10.1080/01614940.2022.2072450
20. Qamar, O. A.; Jamil, F.; Hussain, M.; Bae, S.; Inayat, A.; Shah, N. S.; Waris, A.; Akhter, P.; Kwon, E. E.; Park, Y.-K. *Chem. Eng. J.* **2023,** *460,* 141734. doi:10.1016/j.cej.2023.141734
21. Chen, S.; Hu, Y. H. *Catal. Rev.: Sci. Eng.* **2023,** 1–41. doi:10.1080/01614940.2023.2169451
22. Rafique, M.; Hajra, S.; Irshad, M.; Usman, M.; Imran, M.; Assiri, M. A.; Ashraf, W. M. *ACS Omega* **2023,** *8,* 25640–25648. doi:10.1021/acsomega.3c00963
23. Li, X.; Li, C.; Xu, Y.; Liu, Q.; Bahri, M.; Zhang, L.; Browning, N. D.; Cowan, A. J.; Tang, J. *Nat. Energy* **2023,** *8,* 1013–1022. doi:10.1038/s41560-023-01317-5
24. Wang, Z.; Zhang, Z.; Wang, Z.; Lu, H.; Wang, L. *Appl. Catal., A* **2023,** *654,* 119082. doi:10.1016/j.apcata.2023.119082
25. Meng, L.; Chen, Z.; Ma, Z.; He, S.; Hou, Y.; Li, H.-H.; Yuan, R.; Huang, X.-H.; Wang, X.; Wang, X.; Long, J. *Energy Environ. Sci.* **2018,** *11,* 294–298. doi:10.1039/c7ee02951a
26. Jiang, W.; Low, J.; Mao, K.; Duan, D.; Chen, S.; Liu, W.; Pao, C.-W.; Ma, J.; Sang, S.; Shu, C.; Zhan, X.; Qi, Z.; Zhang, H.; Liu, Z.; Wu, X.; Long, R.; Song, L.; Xiong, Y. *J. Am. Chem. Soc.* **2021,** *143,* 269–278. doi:10.1021/jacs.0c10369
27. Lang, J.; Ma, Y.; Wu, X.; Jiang, Y.; Hu, Y. H. *Green Chem.* **2020,** *22,* 4669–4675. doi:10.1039/d0gc01608j
28. Wu, X.; Zhang, H.; Xie, S.; Wang, Y. *Chem Catal.* **2023,** *3,* 100437. doi:10.1016/j.checat.2022.10.013
29. Li, X.; Xie, J.; Rao, H.; Wang, C.; Tang, J. *Angew. Chem., Int. Ed.* **2020,** *59,* 19702–19707. doi:10.1002/anie.202007557
30. Song, S.; Song, H.; Li, L.; Wang, S.; Chu, W.; Peng, K.; Meng, X.; Wang, Q.; Deng, B.; Liu, Q.; Wang, Z.; Weng, Y.; Hu, H.; Lin, H.; Kako, T.; Ye, J. *Nat. Catal.* **2021,** *4,* 1032–1042. doi:10.1038/s41929-021-00708-9
31. Kim, M.; Lee, J.; Je, M.; Heo, B.; Yoo, H.; Choi, H.; Choi, J.; Lee, K. *J. Mater. Chem. A* **2021,** *9,* 2239–2247. doi:10.1039/d0ta10062e
32. Ding, Y.; Zhang, J.; Yang, Y.; Long, L.; Yang, L.; Yan, L.; Kong, W.; Liu, F.; Lv, F.; Liu, J. *Int. J. Hydrogen Energy* **2021,** *46,* 36069–36079. doi:10.1016/j.ijhydene.2021.08.175
33. Zhang, J.; Chen, X.; Bai, Y.; Li, C.; Gao, Y.; Li, R.; Li, C. *J. Mater. Chem. A* **2019,** *7,* 10264–10272. doi:10.1039/c8ta08199a
34. Wang, W.; Huang, X.; Wu, S.; Zhou, Y.; Wang, L.; Shi, H.; Liang, Y.; Zou, B. *Appl. Catal., B* **2013,** *134–135,* 293–301. doi:10.1016/j.apcatb.2013.01.013
35. Liu, T.; Shi, L.; Wang, Z.; Liu, D. *Colloids Surf., A* **2022,** *632,* 127811. doi:10.1016/j.colsurfa.2021.127811
36. Zhao, W.; Jin, Y.; Gao, C. H.; Gu, W.; Jin, Z. M.; Lei, Y. L.; Liao, L. S. *Mater. Chem. Phys.* **2014,** *143,* 952–962. doi:10.1016/j.matchemphys.2013.10.026
37. Kashyap, V.; Kumar, C.; Chaudhary, N.; Saxena, K. *Silicon* **2023,** *15,* 1203–1210. doi:10.1007/s12633-022-02068-w
38. Sawal, M. H.; Jalil, A. A.; Khusnun, N. F.; Hassan, N. S.; Bahari, M. B. *Electrochim. Acta* **2023,** *467,* 143142. doi:10.1016/j.electacta.2023.143142
39. Chandra, A.; Ghosh, S.; Sarkar, R.; Sarkar, S.; Chattopadhyay, K. K. *Chemosphere* **2024,** *352,* 141249. doi:10.1016/j.chemosphere.2024.141249
40. Shao, M.-W.; Shan, Y.-Y.; Wong, N.-B.; Lee, S.-T. *Adv. Funct. Mater.* **2005,** *15,* 1478–1482. doi:10.1002/adfm.200500080
41. Ta, Q. T. H.; Tran, N. M.; Tri, N. N.; Sreedhar, A.; Noh, J.-S. *Chem. Eng. J.* **2021,** *425,* 131437. doi:10.1016/j.cej.2021.131437
42. Tesvara, C.; Yousuf, M. R.; Albrahim, M.; Troya, D.; Shrotri, A.; Stavitski, E.; Karim, A. M.; Sautet, P. *ACS Catal.* **2024,** *14,* 7562–7575. doi:10.1021/acscatal.4c01018
43. Nguyen, T. T. D.; Le, N. C. T.; Nguyen, D.; Huynh, V. T.; Nguyen, L. T. B.; Nguyen, P. T. *Vietnam J. Chem.* **2023,** *61,* 38–44. doi:10.1002/vjch.202300053
44. Masuda, Y.; Kato, K. *J. Ceram. Soc. Jpn.* **2009,** *117,* 373–376. doi:10.2109/jcersj2.117.373
45. Park, Y.-S.; Lee, J. S. *ACS Photonics* **2017,** *4,* 2587–2594. doi:10.1021/acsphotonics.7b01018
46. Elfiad, A.; Benredouane, S.; Naama, S.; Moulai, F.; Friha, S.-E.; Hadjersi, T. *J. Photochem. Photobiol., A* **2024,** *451,* 115503. doi:10.1016/j.jphotochem.2024.115503
47. Vemula, S. K.; Katta, V. S.; Ojha, S.; Singh, F.; Raavi, S. S. K. *Opt. Mater. (Amsterdam, Neth.)* **2024,** *148,* 114947. doi:10.1016/j.optmat.2024.114947
48. Chen, Q.; Wang, Z.; Liao, H.; Li, R.; Feng, Z.; Li, Z.; Lin, L.; Li, J.; Chen, G. *Chem. Eng. J.* **2024,** *493,* 152316. doi:10.1016/j.cej.2024.152316

49. Cai, J.; Wang, Z.; Jia, S.; Feng, Z.; Ren, Y.; Lin, L.; Chen, G.; Zheng, Z. *ACS Appl. Mater. Interfaces* **2022,** *14,* 13703–13712. doi:10.1021/acsami.1c23939
50. Huang, Q.; Cai, J.; Wei, F.; Fan, Y.; Liang, Z.; Liu, K.; Lu, X. F.; Ding, Z.; Wang, S. *J. Mater. Chem. A* **2024,** *12,* 21334–21340. doi:10.1039/d4ta02049a
51. Yu, L.; Shao, Y.; Li, D. *Appl. Catal., B* **2017,** *204,* 216–223. doi:10.1016/j.apcatb.2016.11.039
52. Yu, X.; Zholobenko, V. L.; Moldovan, S.; Hu, D.; Wu, D.; Ordomsky, V. V.; Khodakov, A. Y. *Nat. Energy* **2020,** *5,* 511–519. doi:10.1038/s41560-020-0616-7
53. Yang, X.; Chen, M.; Weng, C.; Zhuge, D.; Jin, F.; Xiao, Y.; Tian, D.; Yin, Q.; Li, L.; Zhang, X.; Shi, G.; Lu, X.; Yan, L.; Wang, L.; Wen, B.; Zhao, Y.; Lin, J.; Wang, F.; Zhang, W.; Chen, Y. *Adv. Sci.* **2024,** *11,* 2470173. doi:10.1002/advs.202470173
54. Somvanshi, D.; Jit, S. *IEEE Trans. Nanotechnol.* **2014,** *13,* 62–69. doi:10.1109/tnano.2013.2290553
55. Tran Huu, H.; Ngo Van, N.; Vo, V.; Nguyen Thi, L. *Vietnam J. Catal. Adsorpt.* **2021,** *10,* 56–62. doi:10.51316/jca.2021.090
56. Rawat, G.; Somvanshi, D.; Kumar, H.; Kumar, Y.; Kumar, C.; Jit, S. *IEEE Trans. Nanotechnol.* **2016,** *15,* 193–200. doi:10.1109/tnano.2015.2512565
57. Sze, S. M.; Li, Y.; Ng, K. K. *Physics of Semiconductor Devices,* 4th ed.; John Wiley & Sons, 2021. doi:10.1002/0470068329
58. Chen, J.-Z.; Chen, T.-H.; Lai, L.-W.; Li, P.-Y.; Liu, H.-W.; Hong, Y.-Y.; Liu, D.-S. *Materials* **2015,** *8,* 4273–4286. doi:10.3390/ma8074273
59. Liu, Y.; Ji, G.; Dastageer, M. A.; Zhu, L.; Wang, J.; Zhang, B.; Chang, X.; Gondal, M. A. *RSC Adv.* **2014,** *4,* 56961–56969. doi:10.1039/c4ra10670a
60. Gulati, S.; Mulvehill, M. C.; Thompson, T. C.; Spurgeon, J. M. *Energy Fuels* **2023,** *37,* 8573–8582. doi:10.1021/acs.energyfuels.3c00568
61. Yao, X.; Chen, L.; Liu, M.; Feng, D.; Wang, C.; Lu, F.; Wang, W.; Wang, X.; Cheng, Y.; Liu, H.; Chen, H.; Wang, W. *Appl. Catal., B* **2018,** *221,* 70–76. doi:10.1016/j.apcatb.2017.08.087

License and Terms